


Synclinc-anticlinc symmetry in the structure of multilayer polar liquid crystals

P. V. Dolganov

Institute of Solid State Physics of the Russian Academy of Sciences, Chernogolovka, Moscow Region, 2 Academician Ossipyan Street, 142432 Russia

 (Received 20 February 2018; revised manuscript received 17 August 2018; published 28 September 2018)

A large number of smectic phases can have the same energy when short-range interlayer interactions (interaction of nearest layers and frustrating next-nearest layer interaction) are taken into account. In this situation even weak long-range interactions become important. They lift the degeneracy and lead to the appearance of a manifold of polar structures with multilayer periodicity. We analyze the reasons for the appearance of six-layer structures observed in experiments. Due to specific symmetry of interlayer interactions each antiferroelectric structure corresponds to a ferroelectric one in which synclinc orientations of molecules in nearest layers are replaced by anticlinc and vice versa. It is shown how different long-range interlayer interactions transform the degeneracy and induce different stable and metastable structures.

DOI: [10.1103/PhysRevE.98.032707](https://doi.org/10.1103/PhysRevE.98.032707)

I. INTRODUCTION

Polar liquid crystals attract substantial attention from researchers due to their unusual structure, polar characteristics, and potential applications [1]. In smectic liquid crystals the molecules are arranged in layers. In the nonpolar SmA phase the molecular long axes are oriented perpendicular to the layer plane. In polar liquid crystals the molecules are tilted with respect to the layer normal. Orientation of molecules in the i th layer can be described by the two-dimensional vector ξ_i oriented in the layer plane (Fig. 1). The modulus of ξ_i characterizes the tilt angle of molecules θ_i , the direction of ξ_i defines the azimuthal orientation of molecules (angle φ_i). Layer polarization is perpendicular to the molecular tilt plane.

Change of the azimuthal and polar orientation of molecules from layer to layer [Fig. 1(b)] form a wide variety of smectic phases. There are two types of qualitatively different polar structures. The SmC_α^* phase is characterized by a short-pitch helix whose period is incommensurate with the layer spacing. The SmC_α^* phase can be formed at temperatures near the transition to the nonpolar SmA phase [1]. The majority of polar phases have commensurate structures with period from one to about 10 molecular layers. In this work commensurate structures are considered. In these phases the change of the azimuthal orientation of molecules from layer to layer $\Delta\varphi_i = \varphi_{i+1} - \varphi_i \approx 0$ or $\Delta\varphi_i \approx \pi$. The difference in $\Delta\varphi_i$ from 0 or π is due to the chirality of molecules, which induces a long-period helix with a pitch on the order of 10^2 – 10^4 smectic layers [2]. Further we will be interested in the short range order of commensurate structures. First we will consider either synclinc ($\Delta\varphi_i = 0$) or anticlinc ($\Delta\varphi_i = \pi$) orientation of molecules in adjacent layers. Then the influence of chiral interaction and nonplanar structure on the stability regions of phases will be discussed.

The discovery of multilayer phases was an important step in studies of polar liquid crystals. The three-layer ferroelectric SmC_{d3}^* and four-layer SmC_{d4}^* , so-called antiphase (Fig. 2), were experimentally observed and are commensurate multi-

layer phases [1,3]. The SmC_{d4}^* phase is considered to form as a result of frustration [1,4]. Theoretical description of these structures was performed employing phenomenological and microscopic approaches [5–13]. In recent years a rich variety of other multilayer polar phases with period N larger than four molecular layers was discovered [14–24]. The greatest interest was inspired by the discovery of six-layer phases in measurements of resonant x-ray scattering [14,16,17]. The authors [14,16–18] identified the discovered structures as the six-layer antiferroelectric $\text{SmC}_{d6/4A}^*$ and ferroelectric $\text{SmC}_{d6/4F}^*$ [Figs. 2(e) and 2(g)]. To avoid confusion, for the six-layer structures we will further use the notation in which the first two subscripts denote the period of the structure, the next subscripts indicate the number of synclinc pairs in the unit cell and the type of the structure: antiferroelectric (A) or ferroelectric (F). Six-layer structures were obtained previously in calculations together with other polar phases [9,25]. However, until now there is no full clarity about the interactions responsible for the emergence of these structures, and whether other six-layer phases can exist.

In this work calculations of the structures with different sets of interlayer interactions were performed using discrete Landau theory of phase transitions with two-component order parameter. Long-range interactions were consecutively introduced in the free energy. It was established which interactions are responsible for appearance of different phases. It is shown that besides the experimentally observed $\text{SmC}_{d6/4A}^*$ and $\text{SmC}_{d6/4F}^*$ phases (Fig. 2) other structures, including a six-layer phase, can form. Even when long-range (third-nearest neighbor) interactions are taken into account, the energy of a number of structures remains degenerate, which can lead to appearance of disordered structures.

II. RESULTS

In the Landau theory of phase transitions used to describe polar phases [1,12], the order parameter can be the two-dimensional vector ξ_i . Free energy is written in the form

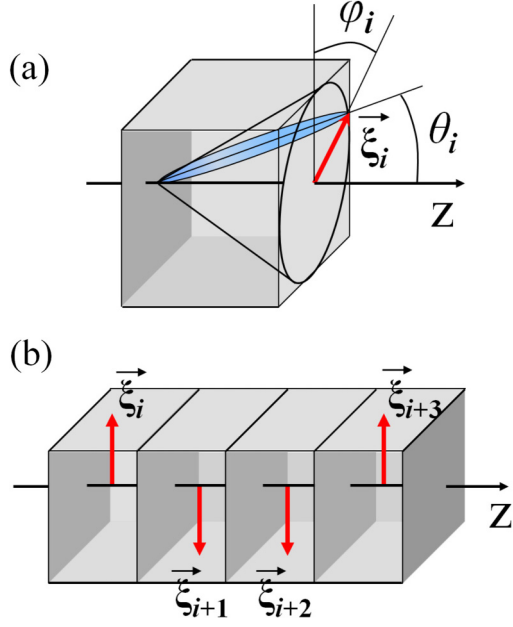


FIG. 1. (a) Two-component vector ξ_i characterizes the polar (angle θ_i) and azimuthal (angle φ_i) orientation of molecules in i th smectic layer. (b) Multilayer polar phases are formed by change of the orientation of ξ_i from layer to layer.

$F = F_1 + F_2$, where F_1 describes the orientational ordering in noninteracting smectic layers

$$F_1 = \sum_i \left[\frac{1}{2} \alpha (T - T^*) \xi_i^2 + \frac{1}{4} b_0 \xi_i^4 \right], \quad (1)$$

T^* is the temperature of the transition to nonpolar SmA phase in absence of interlayer interactions. F_2 includes the interaction between nearest layers and the long-range interactions between next-nearest, second-nearest, third-nearest layers

$$F_2 = \frac{1}{2} a_1 \sum_i \xi_i \cdot \xi_{i+1} + \frac{1}{8} a_2 \sum_i \xi_i \cdot \xi_{i+2} + a_3 \sum_i \xi_i \cdot \xi_{i+3} + a_4 \sum_i \xi_i \cdot \xi_{i+4}. \quad (2)$$

Interactions between layers are related to steric and van der Waals interaction between nearest layers and effective longer range indirect interaction. The origin of the long-range interaction up to the fourth-nearest layers was considered in detail in the work of Čepič *et al.* [8,26]. The physical reasons for the long-range interaction are flexoelectric and electrostatic dipolar interaction. The free energy depends on the structure ξ_i and polar η_i order parameters [8,26]. Minimization of the free energy with respect to η_i gives an expression for the energy which depends only on ξ_i . In this expression long-range interlayer interactions (between next-nearest layers and interactions of longer range) appear in the free energy. They are proportional to the ratio μ^2/\tilde{b}_0 , where μ determines the magnitude of the flexoelectric energy $1/2\mu(\xi_{i+1} - \xi_{i-1}) \cdot \eta_i$ and \tilde{b}_0 corresponds to the polar energy of layers $1/2\tilde{b}_0\eta_i^2$ [8]. The second-nearest and third-nearest layer interactions

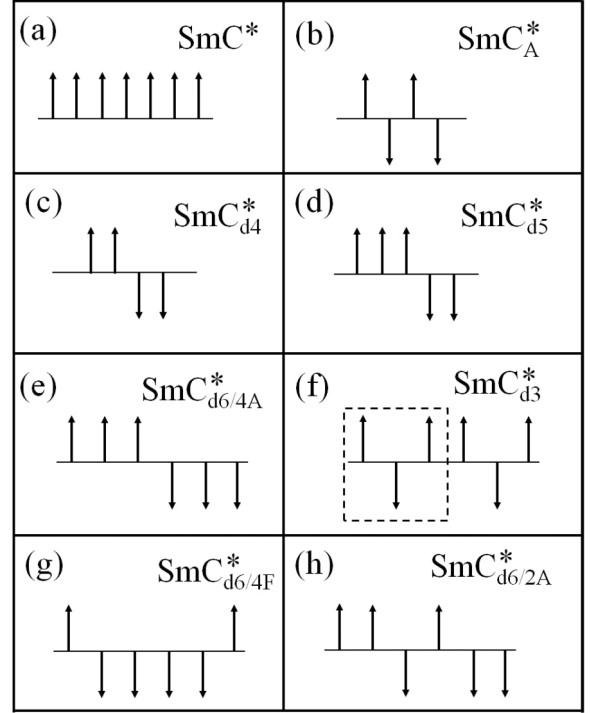


FIG. 2. Orientations of ξ_i in polar phases SmC^* , SmC_A^* , SmC_{d4}^* , SmC_{d5}^* , $\text{SmC}_{d6/4A}^*$, SmC_{d3}^* , $\text{SmC}_{d6/4F}^*$, and $\text{SmC}_{d6/2A}^*$. SmC_{d3}^* and $\text{SmC}_{d6/2A}^*$ structures can be obtained from $\text{SmC}_{d6/4A}^*$ and $\text{SmC}_{d6/4F}^*$ by changing synclinic orientations in nearest layers to anticlinic and vice versa. The rectangle in Fig. 2(f) shows the period of the SmC_{d3}^* phase.

with coefficients a_3 and a_4 depend additionally on parameters describing the electrostatic interaction between nearest and next-nearest layers [8]. The physical order of magnitude of b_0 for tilted smectic structures is about 10^3 kJ/m^3 [27,28]. Other parameters are scaled by b_0 and can be obtained by multiplying a_i by b_0 . In our flat model the tilt direction changes from layer to layer by 0 or π . Calculations of the temperature sequences of commensurate multilayer phases, carried by our group [29] using an analogous model, correspond to experimentally observed sequences. It is worth noting that at present, to the best of our knowledge, these are the only calculations describing the experimentally observed sequences of multilayer phases including different six-layer structures $\text{SmC}_{d6/4A}^*$ and $\text{SmC}_{d6/4F}^*$. The results of these calculations and their agreement with experiment support the validity of the employed model for calculation of transitions between different commensurate phases. The uniplanar model is also used by other groups in the calculations of structures and the intensity of resonant x-ray scattering for 6-layer structures (see Refs. [17,30]). In our calculations the multilayer polar phases do not form a Devil's staircase [4].

The influence of chirality and nonplanar structure on the phase diagrams is discussed in Sec. III. In calculations of nonplanar structures the free energy besides the terms present in Eqs. (1) and (2) contained the Lifshitz term $f[\xi_i \times \xi_{i+1}]_z$ and biquadratic term $b[\xi_i \times \xi_{i+1}]^2$. In nonplanar model the

free energy becomes $F_1 + F_2 + F_3$, where

$$F_3 = f \sum_i [\xi_i \times \xi_{i+1}]_z + b \sum_i [\xi_i \times \xi_{i+1}]^2. \quad (3)$$

The first term in Eq. (3) arises in particular from the chiral part of the van der Waals interaction [8]. Chiral interaction makes structures of commensurate phases nonplanar [1]. The last term in the free energy Eq. (3) is the barrier between the parallel and antiparallel orientations of ξ_i [26]. Its origin was discussed in Refs. [1,26]. We consider commensurate structures at low temperatures, when the influence of the biquadratic interaction is increased.

Minimization of the free energy F was performed over the order parameter ξ_i for various commensurate structures with different orientations of ξ_i and their energies were compared [9,12,31,32]. In the uniplanar (lock-in) model the orientations of ξ_i in nearest layers are synclinic or anticlinic. The structure with the minimal energy for given values of a_i is the stable one. To clarify the influence of chirality and nonplanar structure on the phase diagrams, energy minimization was performed not only over the modulus of the order parameter but also over relative angles $(\varphi_{i+1} - \varphi_i)$ between azimuthal orientations of ξ_i in neighboring layers. In these calculations we used the free energy $F_1 + F_2 + F_3$. The stability regions of different structures calculated in the framework of planar and nonplanar models are presented in Secs. II and III. As demonstrated in experiments carried by different groups, in the majority of compounds the tilt is constant along the structures. For this class of compounds energy minimization is performed with the constant magnitude of the tilt angle. In our calculations in this work $|\xi_i|$ was taken as the same in different layers.

Let us start from the simplest case when only nearest and next-nearest layers interact [the first two terms in Eq. (2)]. We consider the structures at low temperature when commensurate phases are formed. Nearest layer interaction promotes synclinic orientation of molecules [ferroelectric ordering, SmC^* , Fig. 2(a)] for $a_1 < 0$ and anticlinic orientation [antiferroelectric ordering, SmC_A^* , Fig. 2(b)] for $a_1 > 0$. The next-nearest layer interaction [the second term in Eq. (2)] for $a_2 > 0$ favors anticlinic orientation in i th and $(i+2)$ th layers, which is incompatible both with ferroelectric and antiferroelectric structures. A sufficiently strong next-nearest layer interaction $a_2 > 2|a_1|$ leads to frustration [1], which can be released by forming the so-called antiphase SmC_{d4}^* [Fig. 2(c)]. The set of SmC^* , SmC_A^* , SmC_{d4}^* phases and their energies is the starting point for further analysis of multilayer structures. Figure 3 shows energies per layer F_0 for different structures as functions of a_1/a_2 at a fixed temperature. The solid lines give the energies of stable phases. For interlayer interactions quadratic in ξ_i the ranges of phase stability do not change qualitatively with temperature.

A nontrivial peculiarity of the dependence of the energy on a_1/a_2 (Fig. 3) is the existence of global degeneracy points at $|a_1/a_2| = 0.5$. In these points the energies of a large number of structures coincide (energies of several structures passing through the degeneracy points at $|a_1/a_2| = 0.5$ are plotted in Fig. 3 by dotted and dash dotted lines). For example, at $a_1/a_2 = -0.5$ the five-layer SmC_{d5}^* phase [Fig. 2(d)] has the same energy as SmC^* and SmC_{d4}^* . At $a_1/a_2 = 0.5$ the

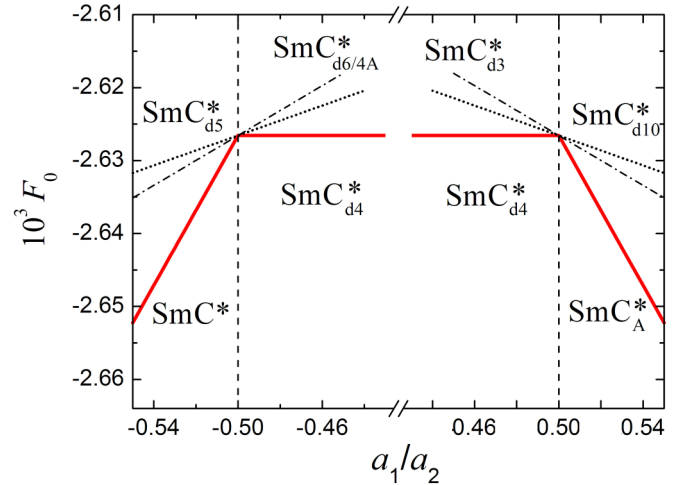


FIG. 3. Dependencies of the energies per layer F_0 on a_1/a_2 for SmC^* , SmC_A^* , and SmC_{d4}^* phases (solid curves). $|a_1/a_2| = 0.5$ are the global degeneracy points in which energies of a large number of phases coincide. The dependencies of energy of several phases on a_1/a_2 passing through the degeneracy points $|a_1/a_2| = 0.5$ are given in the figure. Model parameters: $\alpha = 0.01 \text{ K}^{-1}$, $T - T^* = -10 \text{ K}$, $b_0 = 1$, $a_2 = 0.01$.

ten-layer SmC_{d10}^* phase [33] has the same energy as SmC_A^* and SmC_{d4}^* . With such global degeneracy even a small modification of the interactions could lead to a substantial change in the phase diagrams, since some of the structures become energetically favorable. One of the ways to eliminate degeneracy is the change of the order parameter modulus from layer to layer, which decreases the energy of a number of structures. In the framework of the Landau theory of phase transitions this situation was considered previously [9,32,34]. $\text{SmC}_{d6/4A}^*$ (for $a_1 < 0$) and SmC_{d3}^* (for $a_1 > 0$) become energetically preferable in the vicinity of points $|a_1/a_2| = 0.5$. Modulation of $|\xi_i|$ leads to a possibility of nonresonant x-ray diffraction at wave vectors $q = 2\pi/d(1 \pm m/N)$, where d is the smectic layer thickness and m is an integer. Such nonresonant diffraction was indeed observed in the SmC_{d3}^* phase [35]. The Ising model, which is widely used for the description of magnetic phases, also shows stabilization of $\text{SmC}_{d6/4A}^*$ and SmC_{d3}^* structures [36]. Another possible reason for their stabilization is related to the features of bending fluctuations of smectic layers [11,37]. Anisotropy of layer stiffness with respect to orientation of ξ can lead to correlated ordering of tilt planes in different layers and result in periodic commensurate structures. There are also other reasons for lifting the global degeneracy at $|a_1/a_2| = 0.5$.

First we consider the uniplanar structures and influence of long-range interactions, Eq. (2), on the appearance of multilayer phases. An effective interaction of second-nearest layers and interactions of longer range arise in particular due to polarity of smectic layers and the flexoelectric effect [1,8,26]. Let us start the discussion from the part of the phase diagram with the ferroelectric SmC^* phase, Fig. 3 ($a_1/a_2 < 0$). Long-range interactions induce two types of structures. When the interaction of second-nearest layers $a_3(\xi_i \cdot \xi_{i+3})$ with a positive value of the parameter a_3 is present, the antiferroelectric $\text{SmC}_{d6/4A}^*$ phase [Fig. 2(e)] becomes

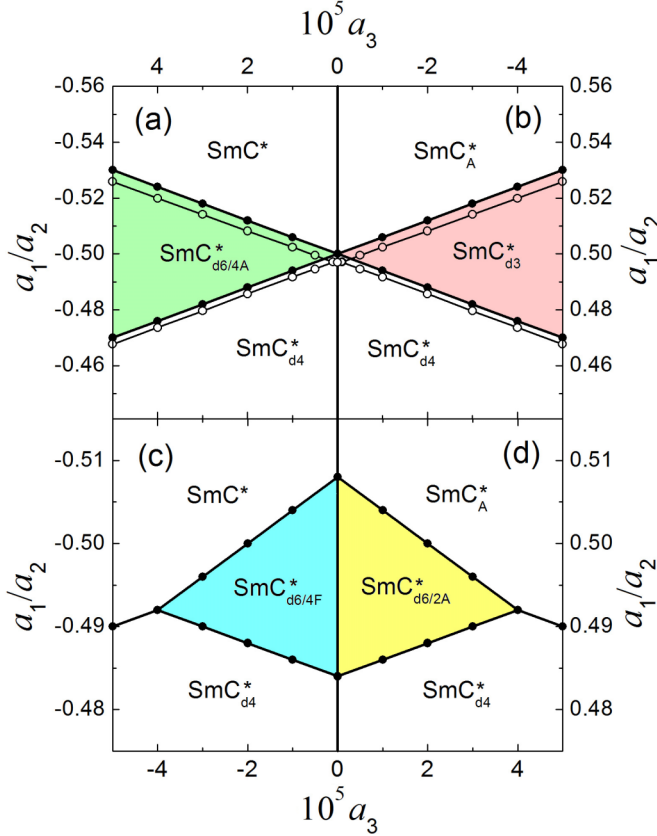


FIG. 4. Stability regions of $\text{SmC}_{d6/4A}^*$ (a), SmC_{d3}^* (b), $\text{SmC}_{d6/4F}^*$ (c), and $\text{SmC}_{d6/2A}^*$ (d) phases in the parameter space of interlayer interactions (a_3 , a_1/a_2). Model parameters: $\alpha = 0.01 \text{ K}^{-1}$, $T - T^* = -10 \text{ K}$, $b_0 = 1$, $a_2 = 0.01$, $a_4 = 0$ (a), (b); $a_4 = 2 \times 10^{-5}$ (c), (d). Solid points show the results of calculations for uniplanar structures. Open points in (a),(b) illustrate the influence of chiral interaction on the phase diagram. Calculations for nonplanar structures were performed with parameters $f = 0.002$, $b = 0.09$. The upper horizontal axis stands for (a),(b), the lower axis for (c), (d).

stable. The second-nearest layer interaction with $a_3 > 0$ favors the $\text{SmC}_{d6/4A}^*$ phase because in this phase ξ_i and ξ_{i+3} for all i are antiparallel [see Fig. 2(e)] and the corresponding contribution to the energy is negative. The stability region of the $\text{SmC}_{d6/4A}^*$ phase is given in Fig. 4(a) in parameter space (a_3 , a_1/a_2). The stability range of $\text{SmC}_{d6/4A}^*$ increases with increasing a_3 . The boundary between $\text{SmC}_{d6/4A}^*$ and SmC_{d4}^* phases [thick solid line in Fig. 4(a)] is the degeneracy line, on which the five-layer ferroelectric SmC_{d5}^* structure exists. So the interaction of second-nearest layers lifts the degeneracy with respect to the $\text{SmC}_{d6/4A}^*$ phase, but degeneracy with respect to SmC_{d5}^* remains. The dependence of energy F_0 of phases on a_1/a_2 for $a_3 = 3 \times 10^{-5}$ is shown in Fig. 5. The $\text{SmC}_{d6/4A}^*$ phase is stable for $-0.518 < a_1/a_2 < -0.482$ and metastable outside this range. The SmC^* phase becomes stable for $a_1/a_2 < -0.518$, the SmC_{d4}^* phase becomes stable for $a_1/a_2 > -0.482$. At $a_1/a_2 = -0.482$ the energy of $\text{SmC}_{d6/4A}^*$ and SmC_{d4}^* phases is equal to the energy of the SmC_{d5}^* phase (open symbols in Fig. 5). In other regions in Fig. 5 the SmC_{d5}^* phase is metastable. SmC_{d3}^* and SmC_{d10}^* phases are metastable in the whole range of Fig. 5. Their

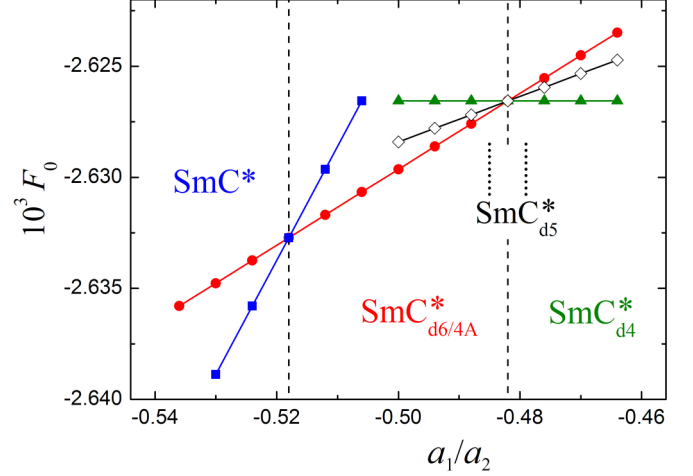


FIG. 5. Dependence of the energies per layer F_0 on a_1/a_2 for SmC^* (solid squares), $\text{SmC}_{d6/4A}^*$ (solid circles), SmC_{d4}^* (solid triangles), and SmC_{d5}^* (open diamonds). Vertical dashed lines border stability ranges of the SmC^* , $\text{SmC}_{d6/4A}^*$, and SmC_{d4}^* phases. Model parameters: $\alpha = 0.01 \text{ K}^{-1}$, $T - T^* = -10 \text{ K}$, $b_0 = 1$, $a_2 = 0.01$, $a_3 = 3 \times 10^{-5}$, $a_4 = 0$. The short dotted lines show the stability range of the SmC_{d5}^* phase with the fourth-nearest layer interaction $a_5 = -3 \times 10^{-6}$.

energies are sufficiently larger, for example at the point $a_1/a_2 = -0.5$ the energy F_0 is about -2.46×10^{-3} for the SmC_{d3}^* phase and about -2.52×10^{-3} for the SmC_{d10}^* phase. The interaction between third-nearest layers $a_4(\xi_i \cdot \xi_{i+4})$ also does not lift the degeneracy of the SmC_{d5}^* phase at the boundary of SmC_{d4}^* and $\text{SmC}_{d6/4A}^*$. This degeneracy can be lifted by including in the free energy the interaction between fourth-nearest layers $a_5(\xi_i \cdot \xi_{i+5})$. The interaction with $a_5 > 0$ makes the SmC_{d5}^* structure unfavorable since ξ_i and ξ_{i+5} in this phase are parallel for all i and the contribution of fourth-nearest layers interaction into the energy is positive. On the boundary between SmC_{d4}^* and $\text{SmC}_{d6/4A}^*$ phases the SmC_{d5}^* structure becomes metastable with respect to four-layer and six-layer phases. If $a_5 < 0$ the SmC_{d5}^* becomes the stable phase in some range between SmC_{d4}^* and $\text{SmC}_{d6/4A}^*$. In particular, for $a_5 = -3 \times 10^{-6}$ the SmC_{d5}^* phase is stable in the range $-0.485 < a_1/a_2 < -0.479$ (vertical dotted lines in Fig. 5). To the best of our knowledge, until now there is no information about the sign of a_5 . Experimental observation of the SmC_{d5}^* structure [15] suggests that a_5 could be negative.

If $a_3 < 0$, the antiferroelectric six-layer phase does not form. However, if the interaction of third-nearest layers $a_4(\xi_i \cdot \xi_{i+4})$ is taken into account, for $|a_3| < 2a_4$ the ferroelectric $\text{SmC}_{d6/4F}^*$ phase [Fig. 2(g)] becomes stable. The stability region of this phase is given in Fig. 4(c) for $a_4 = 2 \times 10^{-5}$. It is worth noting that for $a_4 > 0$ the third-nearest layer interaction in equal manner stabilizes both six-layer structures $\text{SmC}_{d6/4A}^*$ and $\text{SmC}_{d6/4F}^*$. The contribution of the interaction to the energy of these structures per layer is the same and equals $-1/3a_4|\xi|^2$. Figures 6(a) and 6(b) show the stability regions of $\text{SmC}_{d6/4F}^*$ and $\text{SmC}_{d6/4A}^*$ structures in the parameter space of long-range interactions (a_3 , a_4). For $a_4 > 0$ the vertical axis is the coexistence line of two six-layer phases.

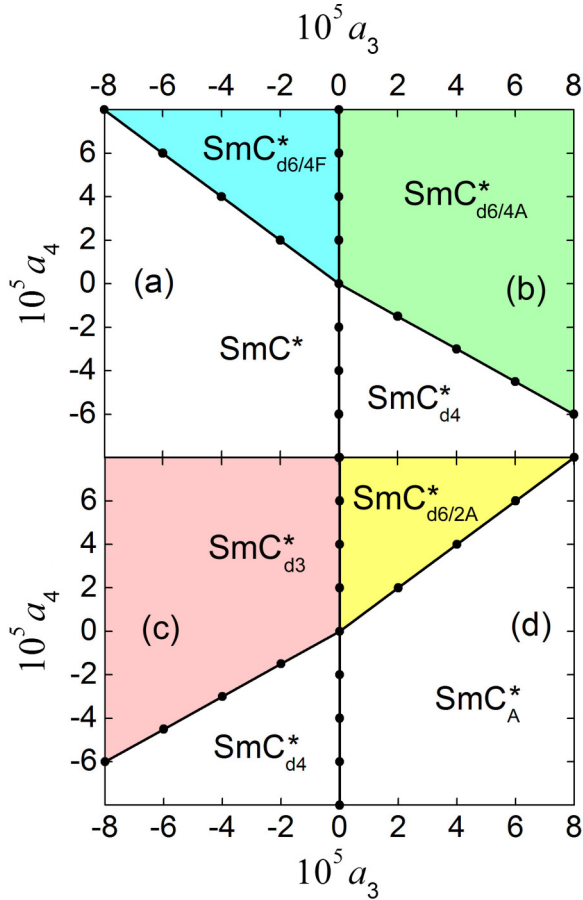


FIG. 6. Stability regions of $\text{SmC}_{d6/4F}^*$ (a), $\text{SmC}_{d6/4A}^*$ (b), SmC_{d3}^* (c), $\text{SmC}_{d6/2A}^*$ (d) phases (uniplanar model) in the parameter space of long-range interactions (a_3 , a_4). $\alpha = 0.01\text{K}^{-1}$, $T - T^* = -10\text{K}$, $b_0 = 1$, $a_2 = 0.01$. $a_1 = -0.005$ (a), (b), $a_1 = +0.005$ (c), (d).

If synclinic orientation in nearest layers is changed to anticlinic and vice versa, $\text{SmC}_{d6/4A}^*$ and $\text{SmC}_{d6/4F}^*$ phases transform into ferrielectric SmC_{d3}^* and antiferroelectric $\text{SmC}_{d6/2A}^*$ structures shown correspondingly in Figs. 2(f) and 2(h). The sequence of six layers that forms from $\text{SmC}_{d6/4A}^*$ comprises two periods of the SmC_{d3}^* phase [Fig. 2(f)]. Precisely the same structures, SmC_{d3}^* and $\text{SmC}_{d6/2A}^*$, form in the right part of the phase diagram in Fig. 3 with the antiferroelectric SmC_A^* phase and positive ratio $a_1/a_2 \approx 0.5$. Stability regions of SmC_{d3}^* and $\text{SmC}_{d6/2A}^*$ structures as function of parameters (a_3 , a_1/a_2) are shown in the right part of Fig. 4. Stability regions in the parameter space of long-range interactions (a_3 , a_4) are shown in Figs. 6(c) and 6(d). For $a_1 < 0$ [Figs. 4(a) and 4(c)] and $a_1 > 0$ [Figs. 4(b) and 4(d)] stability regions of $\text{SmC}_{d6/4A}^*$ and SmC_{d3}^* , $\text{SmC}_{d6/4F}^*$ and $\text{SmC}_{d6/2A}^*$ can be obtained from each other by mirror reflection with respect to the vertical axis. The reason is that if in $\text{SmC}_{d6/4A}^*$ and $\text{SmC}_{d6/4F}^*$ phases synclinic orientation in nearest layers is changed to anticlinic and vice versa, the energies of nearest- and second-nearest neighbor interactions change sign, and the energies of next-nearest and third-nearest neighbor interactions do not change.

III. DISCUSSION

To date, there have been reports of experimental observation of three (SmC_{d3}^* , $\text{SmC}_{d6/4A}^*$, $\text{SmC}_{d6/4F}^*$) from four (SmC_{d3}^* , $\text{SmC}_{d6/4A}^*$, $\text{SmC}_{d6/4F}^*$, $\text{SmC}_{d6/2A}^*$) structures obtained in calculations. Let us discuss in more detail what may be the reasons behind the appearance of these structures.

Antiferroelectric $\text{SmC}_{d6/4A}^$* [Fig. 2(e)]. Change in the order parameter modulus $|\xi_i|$ from layer to layer [9], fluctuations of smectic layers [11,37], and long-range interactions $a_3(\xi_i \cdot \xi_{i+3})$ can stabilize this structure. It is worth noting that the flexoelectric effect, which is considered as the origin of second-nearest layer interaction, leads to the opposite sign of a_3 [8] than required for the appearance of the $\text{SmC}_{d6/4A}^*$ phase. So stabilization of the $\text{SmC}_{d6/4A}^*$ phase can arise due to modulation of $|\xi_i|$ from layer to layer, fluctuations, or from a different mechanism of second-nearest layer interaction, which leads to $a_3 > 0$. In spite of different mechanisms leading to the appearance of multilayer structures, when long-range interactions or the spatial change of the order parameter modulus are taken into account [38] not only $\text{SmC}_{d6/4A}^*$, but also the five-layer SmC_{d5}^* are observed in both models [33,38]. Moreover, in the model with nearest- and next-nearest layer interactions, when $|\xi_i|$ can change from layer to layer, the degeneracy is lifted [38] and SmC_{d5}^* exists in a narrow range between $\text{SmC}_{d6/4A}^*$ and SmC_{d4}^* .

*Ferrielectric SmC_{d3}^** [Fig. 2(f)]. Different mechanisms can contribute to the appearance of this structure: spatial modulation of $|\xi|$, fluctuations of smectic layers, and long-range interlayer interactions. A negative value of a_3 , which favors the SmC_{d3}^* phase, correlates with the flexoelectric mechanism [8] of the appearance of long-range interlayer interaction $a_3(\xi_i \cdot \xi_{i+3})$. Seemingly due to the combination of different mechanisms, SmC_{d3}^* is observed in numerous compounds. It is worth noting that the combined effect of several mechanisms shifts the boundary of stability region of the SmC_{d3}^* phase (the vertical line in Fig. 6) towards positive a_3 . For $a_1/a_2 = 0.5$, $a_2 = 0.01$ the SmC_{d3}^* phase remains stable up to $a_3/a_1 < 5 \times 10^{-3}$. Since for the stabilization of the SmC_{d3}^* phase in the temperature interval $\sim 1\text{K}$ a small value of the long-range interaction $|a_3/a_1| < 10^{-2}$ is required, several mechanisms of stabilization of the SmC_{d3}^* structure have to be taken into account. An analogous shift occurs at the coexistence line of $\text{SmC}_{d6/4F}^*$ and $\text{SmC}_{d6/4A}^*$ (Fig. 6). The boundary between SmC_{d3}^* and SmC_{d4}^* phases [thick solid line in Fig. 4(b)] is the degeneracy line on which a 10-layer antiferroelectric structure SmC_{d10}^* can exist [33]. The SmC_{d10}^* phase also forms when the order parameter modulus can change from layer to layer [33,38].

Ferrielectric $\text{SmC}_{d6/4F}^$* [Fig. 2(g)]. The phase is formed when the second-nearest and third-nearest layer interactions are present [Fig. 6(a)]. Experimental observation of this structure [17] can be an indication that second-nearest and third-nearest layer interactions are close by magnitude.

Antiferroelectric $\text{SmC}_{d6/2A}^$* (Fig. 2(h), 4(d), 6(d)). Up to now the discovery of this structure has not been reported. Its appearance is the least probable with respect to other considered structures. It can form for positive a_3 (which does not correlate with the flexoelectric mechanism of next-nearest

neighbor interlayer interaction [8]) and for a large value of the third-nearest neighbor interlayer interaction.

Now let us briefly discuss the influence of chiral interaction on the phase diagrams. The free energy [Eqs. (1)–(3)] is used in calculations. We illustrate the influence of chirality on the example of the phase diagram in Figs. 4(a) and 4(b). At high chirality when the period of the SmC_A^* phase is about 50 layers ($f = 0.002$, $b = 0.09$) the point $|a_1/a_2| = 0.5$, $a_3 = 0$ is shifted to smaller $|a_1/a_2|$ values [the open point in Figs. 4(a) and 4(b)]. The stability region of the $\text{SmC}_{d_3}^*$ phase also shifts to smaller a_1/a_2 . The width of the $\text{SmC}_{d_3}^*$ phase somewhat decreases (for $a_3 = -3 \times 10^{-5}$ the width of the stability range of the $\text{SmC}_{d_3}^*$ phase is about 0.036 in the absence of chirality and about 0.034 with chirality). The $\text{SmC}_{d_3}^*$ phase appears for finite a_3 ($a_3 \approx -1 \times 10^{-6}$). An analogous shift occurs for the stability range of the $\text{SmC}_{d_6/4A}^*$ phase [Fig. 4(a)]. These shifts do not induce a qualitative transformation of the phase diagram. We may conclude that a minimal uniplanar

model can be used to describe the main features of the phase diagrams and temperature sequences of the phases.

In this work, analysis of the appearance of multilayer polar smectic phases was performed. It is demonstrated how different interlayer interactions can induce formation of various multilayer structures. Stability regions of six-layer phases were determined in the parameter space of interlayer interactions. The emergence of these phases is related to specific synclinc-anticlinc symmetry of their structures. A change of synclinc orientation in the nearest layers to anticlinc and vice versa leads to transformation of six-layer antiferroelectric structures to ferroelectric. At this transformation the energy does not change if certain interlayer interactions change sign.

ACKNOWLEDGMENT

The reported study was supported in part by RFBR, Grant No. 17-02-00246.

-
- [1] H. Takezoe, E. Gorecka, and M. Čepič, *Rev. Mod. Phys.* **82**, 897 (2010).
 - [2] P. G. de Gennes and J. Prost, *The Physics of Liquid Crystals*, 2nd ed. (Clarendon, Oxford, 1994).
 - [3] $\text{SmC}_{d_3}^*$ and $\text{SmC}_{d_4}^*$ phases are also named in literature SmC_{F11}^* and SmC_{F12}^* .
 - [4] A. Fukuda, Y. Takanishi, T. Isozaki, K. Ishikawa, and H. Takezoe, *J. Mater. Chem.* **4**, 997 (1994).
 - [5] M. Čepič and B. Žekš, *Mol. Cryst. Liq. Cryst.* **263**, 61 (1995).
 - [6] A. Roy and N. V. Madhusudana, *Europhys. Lett.* **36**, 221 (1996).
 - [7] M. Gorkunov, S. Pikin, and W. Haase, *JETP Lett.* **72**, 57 (2000).
 - [8] M. Čepič and B. Žekš, *Phys. Rev. Lett.* **87**, 085501 (2001).
 - [9] P. V. Dolganov, V. M. Zhilin, V. K. Dolganov, and E. I. Kats, *Phys. Rev. E* **67**, 041716 (2003).
 - [10] A. V. Emelyanenko and M. A. Osipov, *Phys. Rev. E* **68**, 051703 (2003).
 - [11] M. B. Hamaneh and P. L. Taylor, *Phys. Rev. Lett.* **93**, 167801 (2004).
 - [12] P. V. Dolganov and E. I. Kats, *Liq. Cryst. Rev.* **1**, 127 (2013).
 - [13] M. Rjili, A. Gharbi, T. Othman, and J. P. Mercierou, *Phys. Rev. E* **89**, 022507 (2014).
 - [14] S. Wang, L. D. Pan, R. Pindak, Z. Q. Liu, H. T. Nguyen, and C. C. Huang, *Phys. Rev. Lett.* **104**, 027801 (2010).
 - [15] A. D. L. Chandani, A. Fukuda, S. Kumar, and J. K. Vij, *Liq. Cryst.* **38**, 663 (2011).
 - [16] L. D. Pan, P. Barois, R. Pindak, Z. Q. Liu, B. K. McCoy, and C. C. Huang, *Phys. Rev. Lett.* **108**, 037801 (2012).
 - [17] Y. Takanishi, I. Nishiyama, J. Yamamoto, Y. Ohtsuka, and A. Iida, *Phys. Rev. E* **87**, 050503(R) (2013).
 - [18] L. D. Pan, R. Pindak, and C. C. Huang, *Phys. Rev. E* **89**, 022501 (2014).
 - [19] A. Iida, I. Nishiyama, and Y. Takanishi, *Phys. Rev. E* **89**, 032503 (2014).
 - [20] Y. Takanishi, Y. Ohtsuka, Y. Takanishi, S. Kano, and A. Iida, *Europhys. Lett.* **109**, 56003 (2015).
 - [21] C. C. Huang, S. Wang, L. Pan, P. Barois, and R. Pindak, *Mol. Cryst. Liq. Cryst.* **610**, 23 (2015).
 - [22] A. Iida, Y. Takanishi, A. Fukuda, and J. K. Vij, *Phys. Rev. E* **94**, 052703 (2016).
 - [23] Z. Feng, A. D. L. Chandani Perera, A. Fukuda, J. K. Vij, K. Ishikawa, A. Iida, and Y. Takanishi, *Phys. Rev. E* **96**, 012701 (2017).
 - [24] A. Iida, Y. Takanishi, A. Fukuda, and J. K. Vij, *Phys. Rev. E* **97**, 062702 (2018).
 - [25] A. V. Emelyanenko and K. Ishikawa, *Soft Matter* **9**, 3497 (2013).
 - [26] M. Čepič, E. Gorecka, D. Pocięcha, B. Žekš, and H. T. Nguyen, *J. Chem. Phys.* **117**, 1817 (2002).
 - [27] I. Abdulhalim and G. Moddel, *Liq. Cryst.* **9**, 493 (1991).
 - [28] P. Archer and I. Dierking, *Eur. Phys. J. E* **18**, 373 (2005).
 - [29] P. V. Dolganov and V. K. Dolganov, *JETP Lett.* **101**, 444 (2015).
 - [30] M. Čepič, *Ferroelectrics* **431**, 13 (2012).
 - [31] P. V. Dolganov, V. M. Zhilin, V. K. Dolganov, and E. I. Kats, *Phys. Rev. E* **82**, 040701(R) (2010).
 - [32] P. V. Dolganov, V. M. Zhilin, V. K. Dolganov, and E. I. Kats, *Phys. Rev. E* **86**, 020701(R) (2012).
 - [33] P. V. Dolganov, *JETP Lett.* **100**, 59 (2014).
 - [34] P. V. Dolganov, V. M. Zhilin, V. E. Dmitrienko, and E. I. Kats, *JETP Lett.* **76**, 498 (2002).
 - [35] P. Fernandes, P. Barois, E. Grelet, F. Nallet, J. W. Goodby, M. Hird, and J.-S. Micha, *Eur. Phys. J. E* **20**, 81 (2006).
 - [36] M. Takeuchi, K. Chao, T. Ando, T. Matsumoto, A. Fukuda, and M. Yamashita, *Ferroelectrics* **246**, 1 (2000).
 - [37] M. B. Hamaneh and P. L. Taylor, *Phys. Rev. E* **75**, 011703 (2007).
 - [38] P. V. Dolganov, V. M. Zhilin, V. K. Dolganov, and E. I. Kats, *Phys. Rev. E* **83**, 061705 (2011).